Estimating Functional Connectivity in MEG Source Imaging

Kensuke Sekihara

Department of Systems Design & Engineering
Tokyo Metropolitan University

Brain functional connectivity analysis
sensor space vs. source space

•There have been numerous interests in estimating functional connectivity in human brain.

•So far, many investigations have been performed using the sensor space analysis, in which a measure of connectivity is computed using sensor data.

•Recently, a growing number of investigations begin to use the source space analysis, which first estimates source activity using an inverse method, and then computes a measure of connectivity using the estimated source activities.

•My talk presents results from our investigations on functional connectivity analysis using MEG source space analysis.

Measures of brain functional connectivity

• Various measures for estimating brain functional connectivity have been proposed.

• The representative measure is the coherence. Phase synchrony measures such as the phase-lag index are a sort of relatives of the coherence measure.

• There are quite a few investigations that use the vector-autoregressive model-based measures such as partial coherence and granger causality.

• More specific model-based approaches such as structural equation modeling or dynamic causal modeling have been applied.

Measures of brain functional connectivity

In our investigation, we use a voxel pair-wise coherence.

In my talk, I restrict myself to the coherence measure, and will talk about applications of several related measures developed based on the coherence measure, such as:

- imaginary coherence,
- envelope imaginary coherence,
- phase-slope index,
- mean imaginary coherence.

Voxel pair-wise coherence measure

The average is computed using epoch/trial averaging

voxel time course

$$\eta_{k,j}(f) = \left| \frac{\left\langle \sigma_k(f)\sigma_j(f)^* \right\rangle}{\sqrt{\left\langle |\sigma_k(f)|^2 \right\rangle \left\langle |\sigma_j(f)|^2 \right\rangle}} \right|, \quad \text{where} \quad \sigma_k(f) = \int s_k(t) e^{-2\pi i f} df$$

voxel spectrum

Voxel pair-wise coherence fundamentally provides six-dimensional information, and such information is difficult to interpret.

Seed coherence:

• When computing voxel coherence, a reference voxel is first determined, and coherence map is computed between this reference voxel, called the seed voxel, and all other voxels.

Seed coherence provides three dimensional information in which interpretation is relatively easy.

Rationale of coherence measure

Lagged cross correlation between the jth- and kth- voxel time courses:

$$R_{j,k}(\tau) = \int s_j(t + \tau) \int s_k(t) dt$$

If $R(\tau)$ is zero for all τ, these two sources are independent.

If $R(\tau)$ is non-zero for some τ, the two sources are considered interacting.

Thus, the squared sum of all the lagged correlations can be a measure of the interaction:

$$\int R_{j,k}(\tau)^2 d\tau = \int \left| \left\langle \sigma_j^m(f) \sigma_k^m(f)^* \right\rangle \right|^2 df \underset{\text{narrow-band signal}}{\longrightarrow} \left| \left\langle \sigma_j^m(f) \sigma_k^m(f)^* \right\rangle \right|^2$$

Magnitude cross-spectrum is equal to the squared sum of all the lagged correlations, and the coherence is the normalized version of this quantity.

Imaginary part of coherence

In MEG source-space coherence analysis, we had better use the imaginary coherence to reduce spurious coherence caused due to algorithm blur (leakage).

Use of the imaginary coherence was proposed by Nolte *et al.* to remove the spurious coherence caused by the volume conduction in EEG sensor-space analysis.

Coherence between the jth and kth voxels:

$$\eta_{j,k}(f) = \Re\left[\eta_{j,k}(f)\right] + i\Im\left[\eta_{j,k}(f)\right]$$
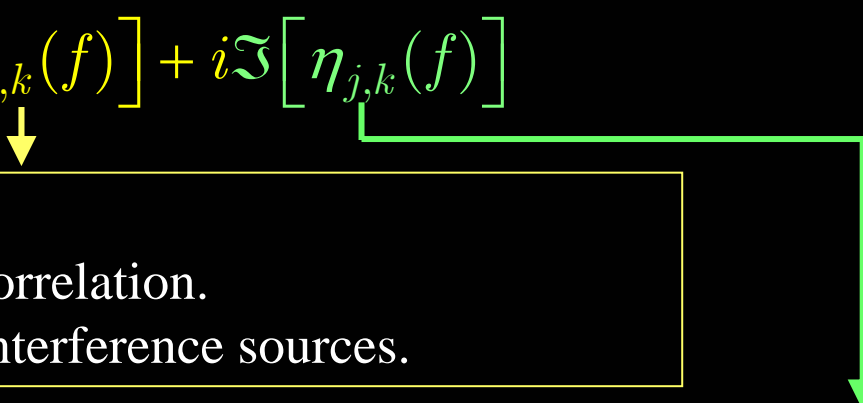
Real part:
- Corresponds to zero time-lag correlation.
- Can be caused from common interference sources.

Imaginary part:
- Corresponds to non-zero time-lag correlation.
- Caused only by true brain interaction.

Imaging imaginary source coherence: computer simulation

Two interacting sources

Source independent from the other two sources

Seed voxel for coherence computation

Magnitude coherence map includes spurious coherence peak caused by the blur of imaging algorithm

The imaginary coherence map does not contain the seed peak, and contains the source that is truly interacting with the seed source.
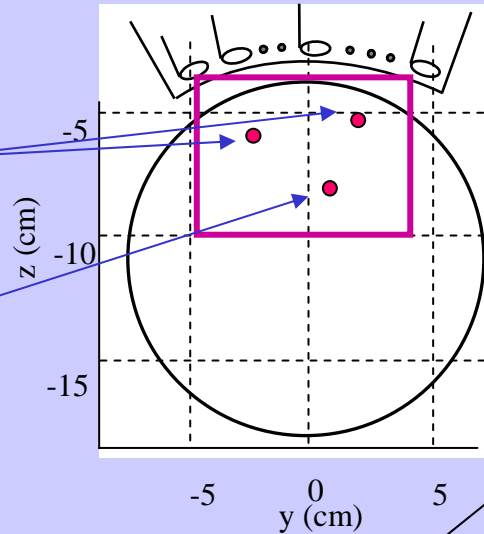
Source image
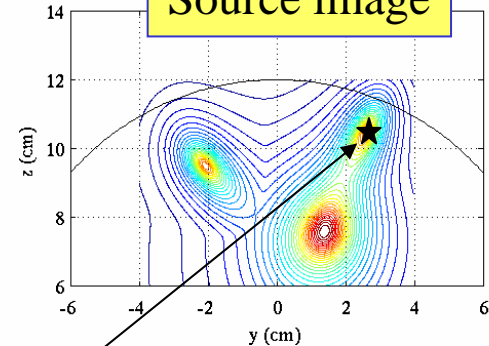
Magnitude coherence

Imaginary coherence

What does imaginary coherence really represent?

Define $\sigma(f)$: target-voxel spectrum; $\sigma_S(f)$: seed-voxel spectrum.

Express $\sigma(f)$ such that $\sigma(f) = \alpha\sigma_S(f) + v(f)$ (α : real number)

The real constant α is determined in the least-squares manner:

$$\hat{\alpha} = \arg\min_{\alpha} \left\langle \left| \sigma(f) - \alpha\sigma_S(f) \right|^2 \right\rangle = \frac{\Re\left[\left\langle \sigma(f)\sigma_S(f)^* \right\rangle\right]}{\left\langle \left| \sigma_S(f) \right|^2 \right\rangle}$$

Therefore, we have:

$$\left\langle v(f)\sigma_S(f)^* \right\rangle = \left\langle \left[\sigma(f) - \hat{\alpha}\sigma_S(f) \right]\sigma_S(f)^* \right\rangle$$

$$= \left\langle \sigma(f)\sigma_S(f)^* \right\rangle - \hat{\alpha}\left\langle \left| \sigma_S(f) \right|^2 \right\rangle = \Im\left[\left\langle \sigma(f)\sigma_S(f)^* \right\rangle\right]$$

Imaginary coherence is actually equal to the coherence between the seed and residual signals; the residual signal is obtained by regressing out the seed signal from the target signal.

Brain MEG signals for measuring functional connectivity

Resting-state coherence

Resting state MEG in the alpha band is used.

Resting state MEG has a relatively high signal-to-interference ratio, and some promising clinical results have been obtained.

Event-related coherence

Induced signal (task-related modulation of oscillatory brain activity), such as ERD or ERS, is used.

Signal-to-interference ratio is low, and a source time-course should be estimated, incorporating the reduction of influence from background interference.

Narrow-band adaptive spatial filter
(used for estimating resting-state coherence)

$\boldsymbol{b}(F_W, t):$ Measured data filtered with frequency band F_W.

$\boldsymbol{R}(F_W):$ Covariance matrix obtained from $\boldsymbol{b}(F_W, t)$.

$\boldsymbol{R}:$ Covariance matrix obtained from broad-band data $\boldsymbol{b}(t)$.

Narrow-band spatial filter:

$$\boldsymbol{w}(F_W, \boldsymbol{r}) = \hat{\boldsymbol{R}}(F_W)^{-1}\,\boldsymbol{l}(\boldsymbol{r})\,/\,[\boldsymbol{l}^T(\boldsymbol{r})\hat{\boldsymbol{R}}(F_W)^{-1}\boldsymbol{l}(\boldsymbol{r})] \quad \text{(narrow-band weight)}$$

$$\hat{s}(\boldsymbol{r}, t) = \boldsymbol{w}^T(F_W, \boldsymbol{r})\boldsymbol{b}(F_W, t)$$

Broad-band spatial filter:

$$\boldsymbol{w}(\boldsymbol{r}) = \hat{\boldsymbol{R}}^{-1}\,\boldsymbol{l}(\boldsymbol{r})\,/\,[\boldsymbol{l}^T(\boldsymbol{r})\hat{\boldsymbol{R}}^{-1}\boldsymbol{l}(\boldsymbol{r})] \qquad\qquad \text{(broad-band weight)}$$

$$\hat{s}(\boldsymbol{r}, t) = \boldsymbol{w}^T(\boldsymbol{r})\boldsymbol{b}(F_W, t)$$

Narrow-band spatial filter can provide spatial resolution much higher than broad-band spatial filter (Sarang et al., NeuroImage, 2008).

Dalal S.S., Guggisberg A.G., Edwards E., Sekihara K., et al., Neuroimage. 2008 May 1;40(4):1686-700.

Brain MEG signals for measuring functional connectivity

Resting state coherence

Resting state MEG, such as alpha rhythm, is used.

Signal-to-noise (interference) ratio is relatively high, and some promising clinical results have been obtained.

Event-related coherence:

Induced signal (task-related modulation of oscillatory brain activity), such as ERD or ERS, is used.

Signal-to-interference ratio is low, and a source time-course should be estimated, incorporating the reduction of influence of baseline activity.

Induced brain signal

Data model: $\boldsymbol{b}(t) = \boldsymbol{b}_S(t) + \boldsymbol{b}_{BL}(t) + \boldsymbol{n}(t)$

measurement   induced signal   baseline activity   sensor noise

For induced signal measurements, dual-condition measurements are, in general, available.

Dual-condition measurements

Task: $\boldsymbol{b}(t) = \boldsymbol{b}_S(t) + \boldsymbol{b}_{BL}(t) + \boldsymbol{n}(t)$

Control: $\boldsymbol{b}_C(t) = \boldsymbol{b}_{BL}(t) + \boldsymbol{n}(t)$

Inverse algorithms should reconstruct source activity only from $\boldsymbol{b}_S(t)$, by making use of $\boldsymbol{b}_C(t)$.

- Prewhitening adaptive spatial filter
- Champagne algorithm

Existing source imaging method that can make use of dual-condition measurements:

Robinson's *F* ratio method: $F(r) = \dfrac{\left\langle s(r)^2 \right\rangle}{\left\langle s_C(r)^2 \right\rangle}$

$s(r)$: source image from $b(t)$

$s_c(r)$: source image from $b_c(t)$

This approach works when SIR is high, but becomes less effective when large baseline activity exists, because the influence of base line activity is not simply additive.

Also, it does not provide source time course, so cannot be used for source coherence estimation in a straight forward manner.

S. E. Robinson and J. Vrba, Recent Advances in Biomagnetism, pp. 302-305, 1999

Prewhitening adaptive spatial filter

Covariance matrix relationship: $\boldsymbol{R} = \boldsymbol{R}_S + \boldsymbol{R}_C$

Task covariance

Control covariance

Covariance from induced signal

$\Rightarrow$ Compute $\tilde{\boldsymbol{R}} = \boldsymbol{R}_C^{-1/2} \boldsymbol{R} \boldsymbol{R}_C^{-1/2}$

Signal covariance estimate

$$\hat{\boldsymbol{R}}_S = \left\langle \boldsymbol{b}_S(t)\boldsymbol{b}_S^T(t) \right\rangle = \boldsymbol{R}_C^{1/2} \left[\boldsymbol{U}_S \boldsymbol{U}_S^T (\tilde{\boldsymbol{R}} - \boldsymbol{I}) \right] \boldsymbol{R}_C^{1/2}$$

$$\boldsymbol{U}_S = [\boldsymbol{u}_1, \ldots, \boldsymbol{u}_Q] : \text{signal-level eigenvectors of } \tilde{\boldsymbol{R}}$$

Signal magnetic-field estimate

$$\hat{\boldsymbol{b}}_S(t) = \boldsymbol{R}_C^{1/2} \boldsymbol{U}_S \boldsymbol{U}_S^T \boldsymbol{R}_C^{-1/2} \boldsymbol{b}(t)$$

Source time-course estimate free from baseline influence

$$\hat{s}(\boldsymbol{r}, t) = \boldsymbol{w}^T(\boldsymbol{r}) \hat{\boldsymbol{b}}_S(t) = \frac{\boldsymbol{l}^T(\boldsymbol{r}) \hat{\boldsymbol{R}}_S^{-1} \hat{\boldsymbol{b}}_S(t)}{\boldsymbol{l}^T(\boldsymbol{r}) \hat{\boldsymbol{R}}_S^{-1} \boldsymbol{l}(\boldsymbol{r})}$$

Sekihara K, et al. IEEE Trans Biomed Eng. 2008 Mar;55(3).

Champagne algorithm

Source imaging based on variational Bayesian technique

Data model: Control: $\boldsymbol{b}_C(t) = \boldsymbol{B}\boldsymbol{u}(t) + \boldsymbol{n}(t)$

Task: $\boldsymbol{b}(t) = \boldsymbol{L}_N\boldsymbol{s}_N(t) + \boldsymbol{B}\boldsymbol{u}(t) + \boldsymbol{n}(t)$

Induced activity   Baseline activity

Two step procedures of Champagne algorithm

(1) The interference mixing matrix $\boldsymbol{B}$ and sensor-noise covariance matrix $\boldsymbol{\Lambda}$ are estimated from the control data:
$\boldsymbol{b}_C(t) = \boldsymbol{B}\boldsymbol{u}(t) + \boldsymbol{n}(t)$.

(2) With $\boldsymbol{B}$ and $\boldsymbol{\Lambda}$, $\boldsymbol{s}_N(t)$ is estimated using the task data:
$\boldsymbol{b}(t) = \boldsymbol{L}_N\boldsymbol{s}_N(t) + \boldsymbol{B}\boldsymbol{u}(t) + \boldsymbol{n}(t)$.

The algorithm is presented in this afternoon for 14:15-14:30 by Julia Owen et al. "Robust Methods for Reconstructing Brain Activity and Functional Connectivity from MEG Data".

Hand-motor MEG data induced by voluntary finger movement

Sensor layout display of time-frequency maps of the data from all sensors

Control

Task

- We set the task and control window in this manner.

- The task window contains beta-band power increase.

Prewhitening narrow-band spatial filter
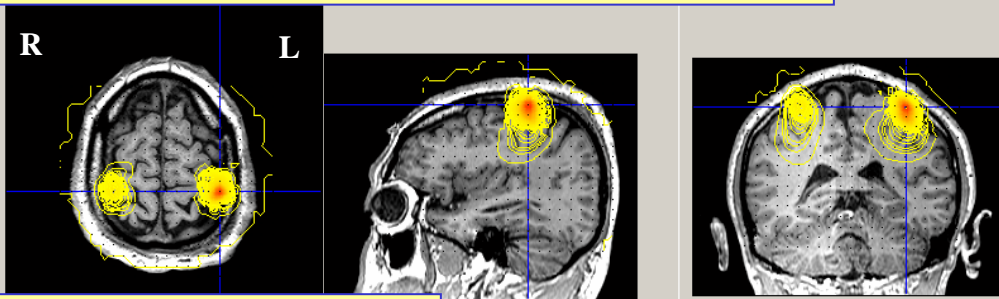
Champagne algorithm
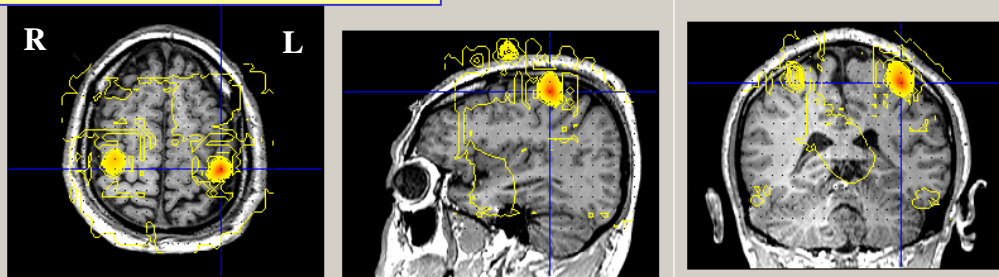
F-image with narrow-band spatial filter
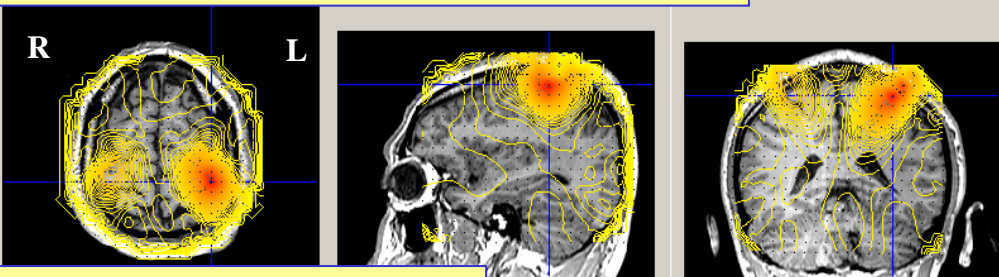
F-image with sLORETA
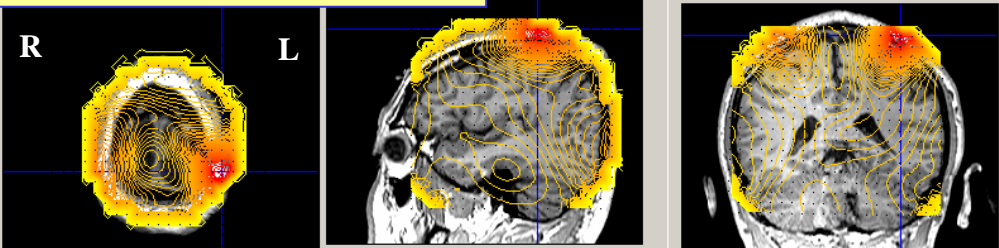
- This slide shows the results of source images obtained using our developed methods and existing methods.

- sLORETA results show some localization bias, and source is not reconstructed at the correct location.

- F-image with narrow-band adaptive spatial filter works fairly well on this data set, because the data contain fairly strong ERD.

- Two developed methods give high spatial resolution, and very small localization bias, so the primary motor cortices in both hemispheres are localized with correct locations.

Coherence imaging of motor-related MEG

Data obtained from subject's right-hand grasping conducted every 15 sec

Sensor-layout display of time-frequency maps
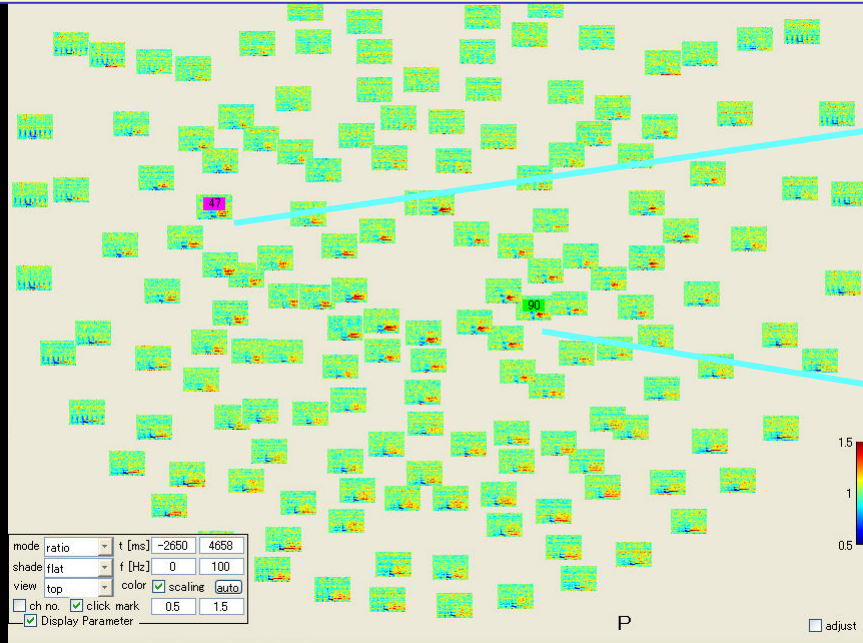
Time-frequency maps for selected sensors
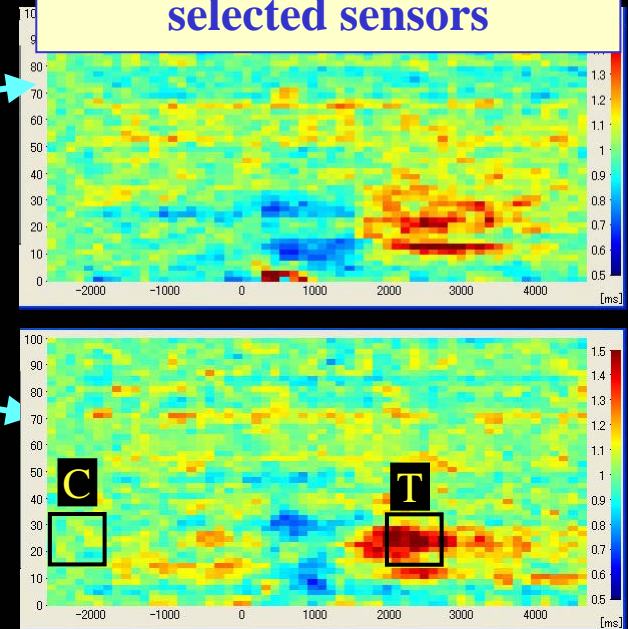
Source image

- Quite strong bilateral beta-band activity around 2-3 sec after the onset of the movements is observed.

- Bilateral motor activation is reconstructed in the results of source reconstruction.
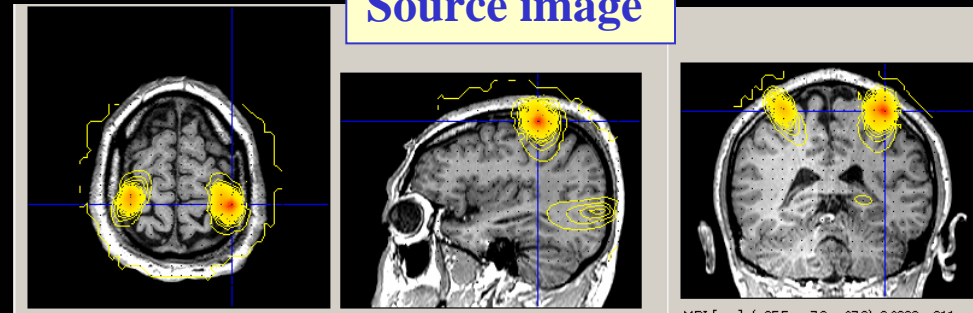
We set a seed point for coherence computation at contra M1.

Source image
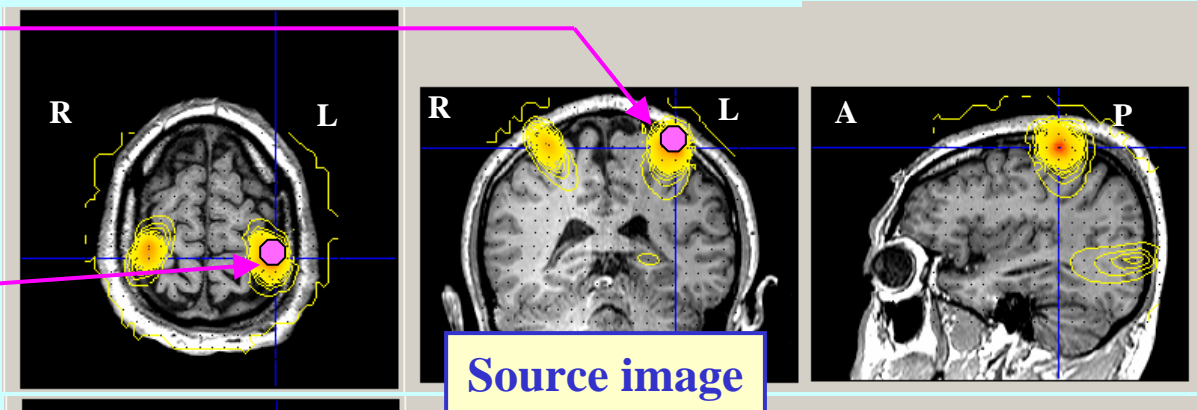
We can only observe the seed blur, which is a spurious coherence peak caused by the blur of imaging algorithm.

Magnitude coherence image
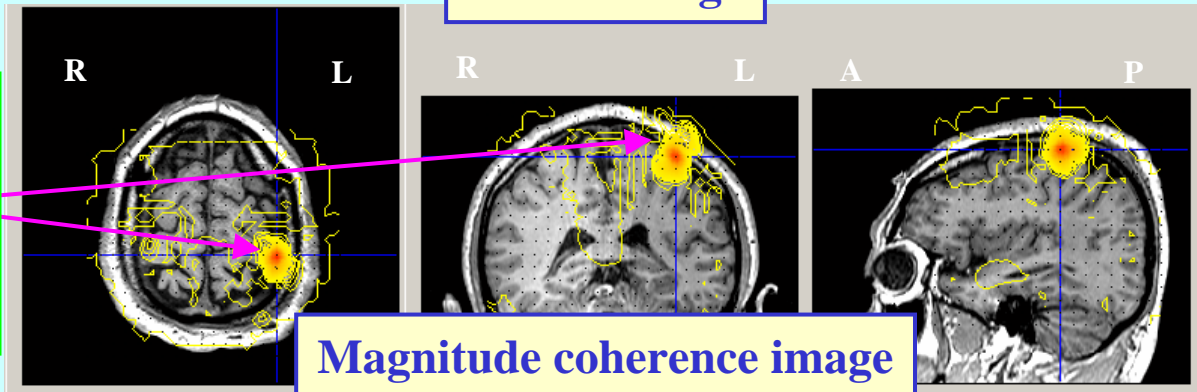
Ipsi M1 is clearly detected with no seed blur peak.

Imaginary coherence image
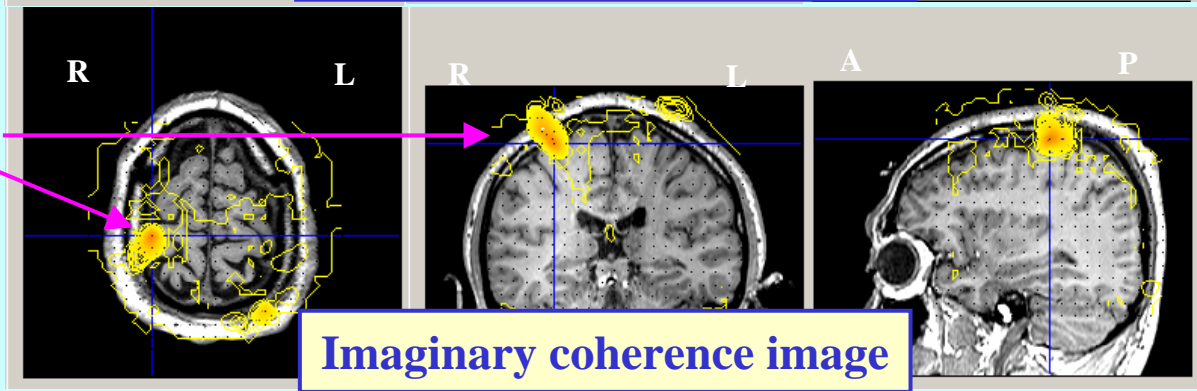
Results show the necessity of imaging imaginary coherence, However, in this particular example, the spurious coherence peak is well separated from the true coherence peak and can be identified by visual inspection.

Imaging source coherence at alpha band
(Resting state MEG from a brain tumor patient)

- Source image shows a large blurred peak in the occipital area.

- The maximum point at this peak is selected as the reference point for the coherence computation.

- The magnitude coherence image is very similar to the source power image, and there is not much information in this magnitude coherence map.

- The imaginary coherence image shows multiple localized sources, and is very different from the magnitude coherence images.

Seed point

Source power image

Magnitude coherence image

Imaginary coherence image
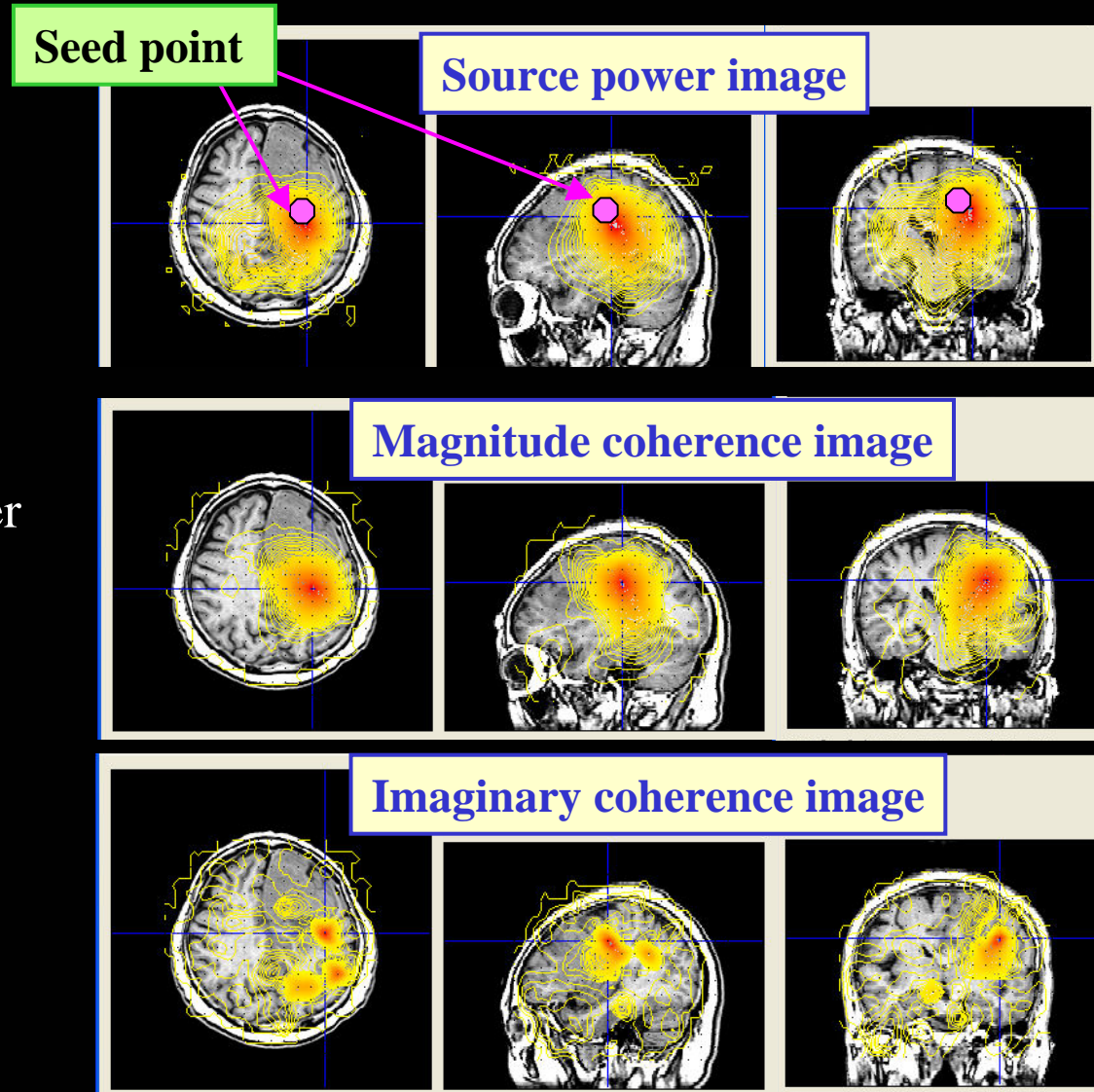
We have not yet explored the clinical relevance of these results. However, the results should indicate potentials of the source imaginary coherence mapping.

Source envelope coherence measure insensitive to inter-source jitters

• Coherence is very sensitive to inter source jitters. This could be more problematic when we deal with high-frequency signal such as high-gamma activity.

• Envelope coherence, computed using the envelopes of estimated source time courses, is considered much robust to inter source jitters.
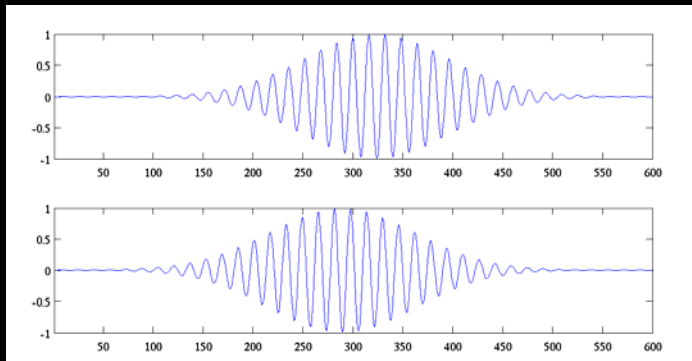
Source time courses   Their envelopes
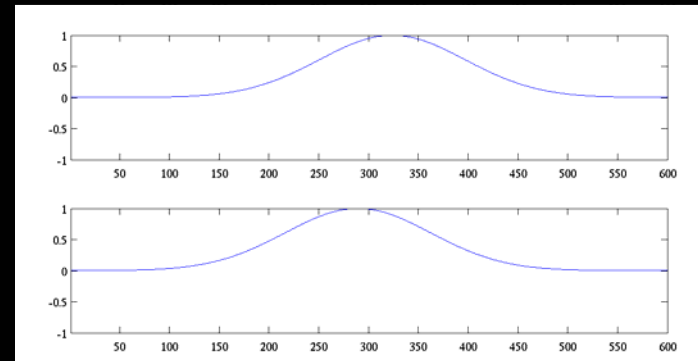
Source time-course envelope is computed using:

$$\hat{\Pi}(t) = \left| \hat{A}(t) \right| = \left| \hat{s}(t) + \frac{i}{\pi} \int \frac{\hat{s}(t')}{t - t'} dt' \right|$$

Analytic signal of $\hat{s}(t)$ Estimated source time course

Results of computing envelope coherence Hand-motor data

Imaginary coherence
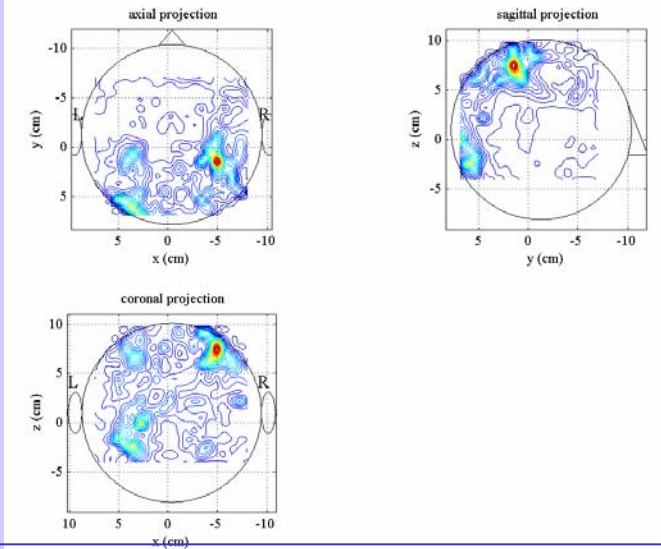
Envelope imaginary coherence
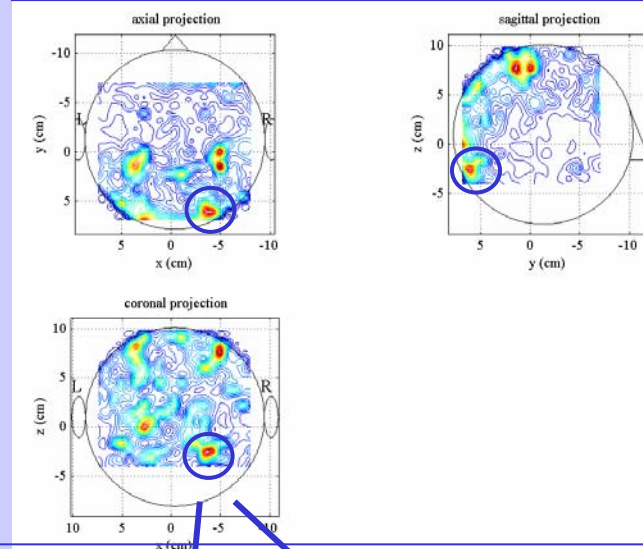
Maximum intensity projection display of coherence 3D mapping results

Two sets of results have the same structural pattern, but envelope coherence results show significantly stronger source activity.
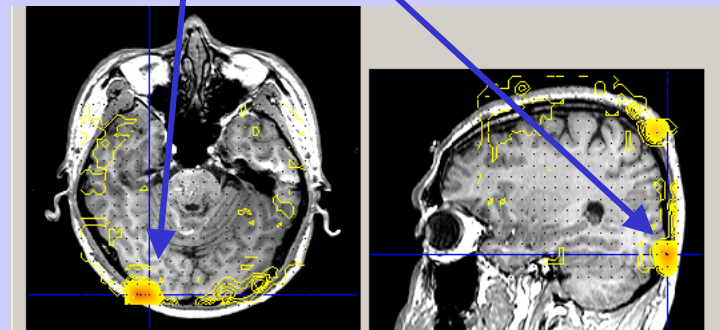
Specifically, the envelope coherence results show quite strong activity near cerebellum.

Estimating direction of information flow using phase-slope index (PSI)

Cross spectrum $\varphi_{j,k} = \left\langle \sigma_j(f)\sigma_k(f)^* \right\rangle$

$\varphi_{j,k} \approx \exp(2\pi i f \tau)$: The phase of $\varphi_{j,k}$ is proportial to f and τ,

where τ is the time needed for information propagating from j to k.

Phase slope: $\dfrac{\partial}{\partial f} \text{phase}(\varphi_{j,k}) \sim \tau$.

Thus, the sign of the phase slope is equal to the sign of τ,
which indicates whether the information flows from j to k or k to j.

The phase slope can be estimated by using the Phase slope index (PSI):

$$\Psi_{j,k} = \Im\left[\sum_{f \in F_w} \varphi_{j,k}(f)^* \varphi_{j,k}(f + \delta f) \right].$$

Here again, we only use the imaginary part of the cross spectrum.

G. Nolte et al.: Phys. Rev. Lett. 100, pp.234101, 2008

Application of PSI to hand-motor MEG data

Source image with **left hand** grasping

Negative PSI image
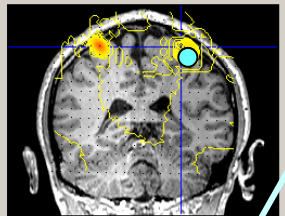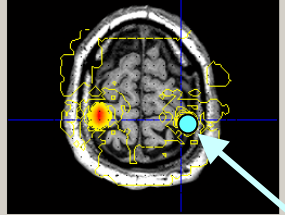
Positive PSI image

Seed a reference point at ipsilateral M1.

Source image with **right hand** grasping
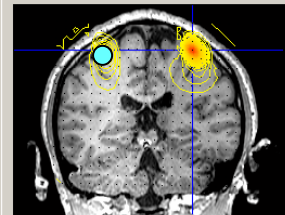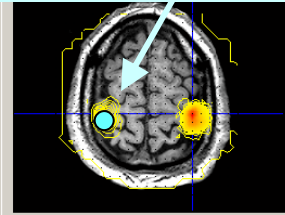
Contra-lateral M1 is detected by negative PSI.

Negative PSI image
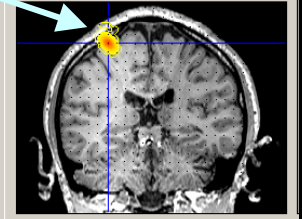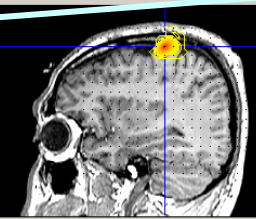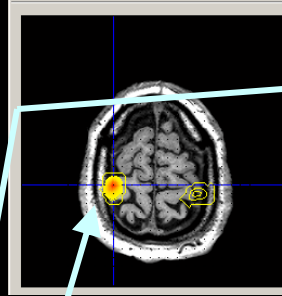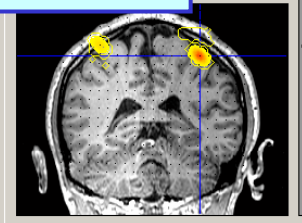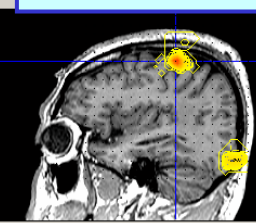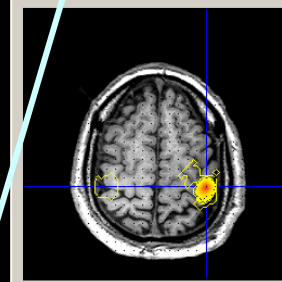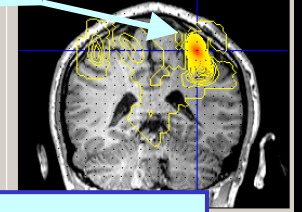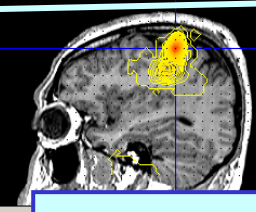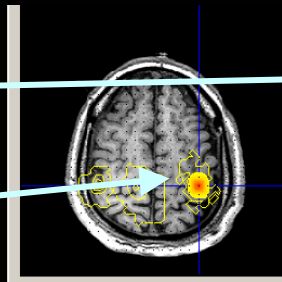
Positive PSI image
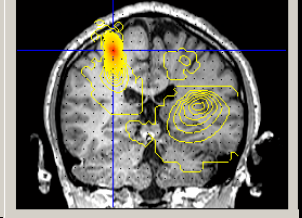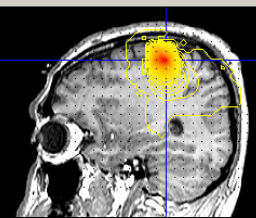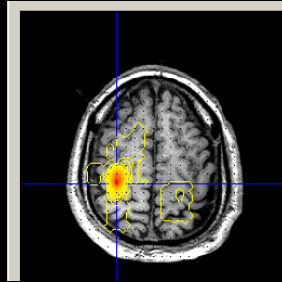
Application of PSI to hand-motor MEG data

Source image with **left hand** movement
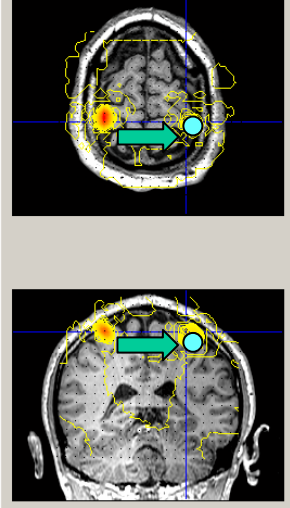
Source image with **right hand** movement
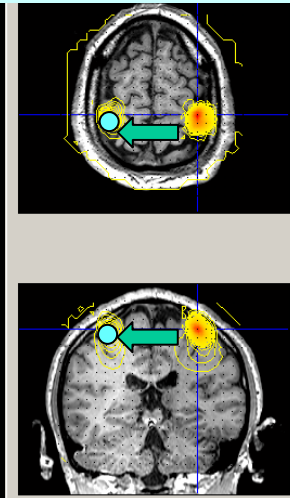
•Thus, these results indicate that the contra-M1 is first activated and the ipsi-M1 is activated later.

•Information flows from the contra-M1 to ipsi-M1.

•Such results agree with our physiological knowledge, and demonstrate the effectiveness of the use of PSI.

So, far my talk is restricted to the seed strategy, in which results are reduced to "interpretable" three dimensional information by introducing a reference (seed) point.

In many applications, however, the determination of the seed location is not a easy task, and may need some a priori knowledge.

Next, I am talking about mean imaginary coherence (MIC), in which the dimensionality of voxel pair-wise coherence is reduced to three dimensions by averaging the estimated imaginary coherence across all voxel pairs.

Mapping of mean imaginary coherence

Coherence between the jth and kth voxels:

$$\eta(f, \boldsymbol{r}_j, \boldsymbol{r}_k) = \alpha(f, \boldsymbol{r}_j, \boldsymbol{r}_k) + i\beta(f, \boldsymbol{r}_j, \boldsymbol{r}_k)$$

Mean imaginary coherence for the jth voxel:

$$\bar{\beta}(f, \boldsymbol{r}_j) = \tanh\left[\frac{1}{K} \sum_{k=1}^{K} \tanh^{-1} |\beta(f, \boldsymbol{r}_j, \boldsymbol{r}_k)| \right]$$

Magnitude value of imaginary coherence is averaged over all voxel connections after the Fisher's Z transform.

$\bar{\beta}(f, \boldsymbol{r}_j)$ is considered to represent average strength of connectivity of brain tissue at $\boldsymbol{r}_j$.

A. G. Guggisberg *et al.*, Annals of Neurology, Sep 25, 2007

Question: "Does mean magnitude coherence also work?"

Some audiences might want to ask a question that mean of magnitude coherence also works.

Mean coherence images from hand-grasping (beta-band) MEG data
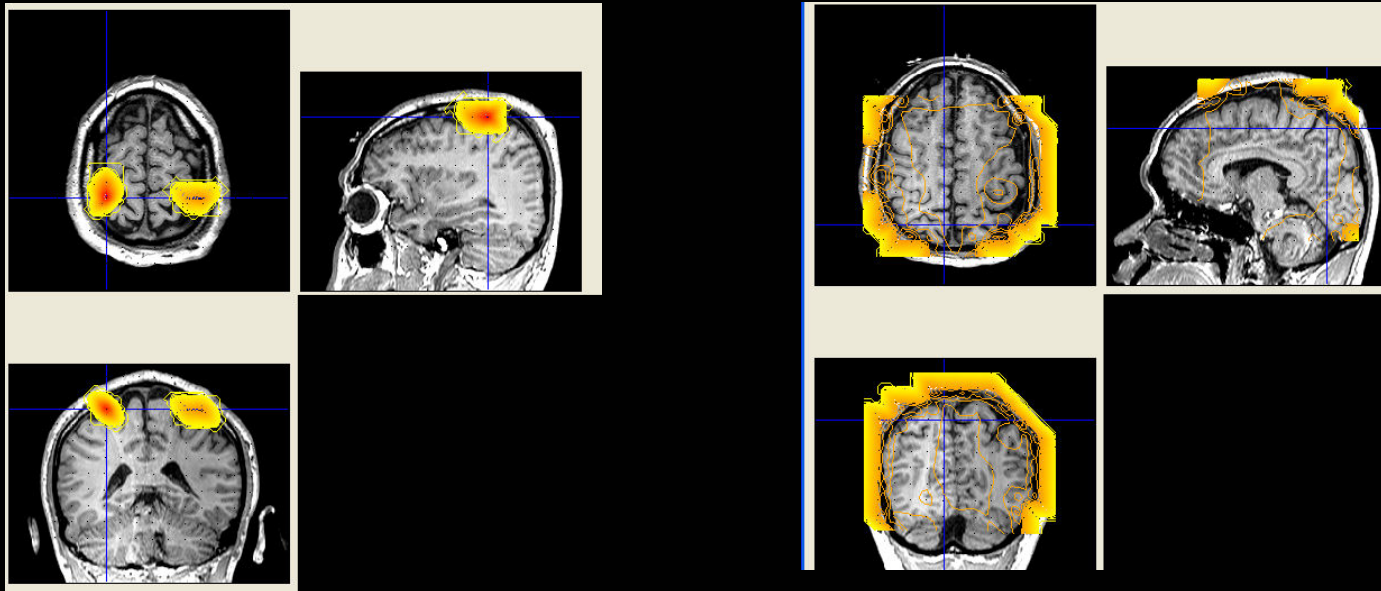
Mean imaginary coherence image   **Mean magnitude coherence image**

- In the mean imaginary coherence image, we can detect the left and the right primary motor areas, as regions that actively communicate with other brain regions.
- Mean magnitude coherence image does not detect these brain regions, and does not provide interpretable results.

Mean imaginary coherence (MIC) image from resting-state (alpha-band) MEG data from a tumor patient

Images below show different MRI slices of MRI overlay results.
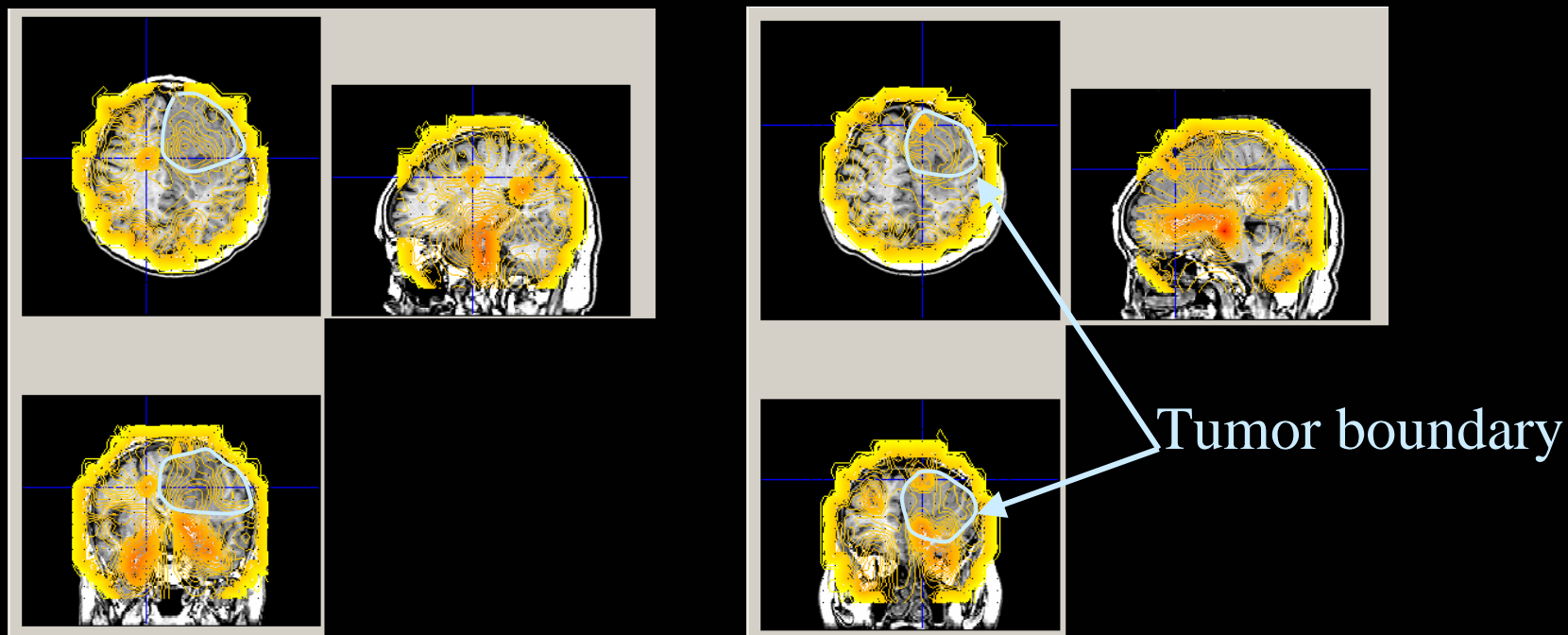
Tumor boundary

The raw results of MIC mapping are difficult to interpret, although some localized regions with high MIC values are found near the tumor boundary.

Statistical significance test of MIC voxel values is necessary.

L-image analysis for patients with unilateral brain tumor

Target voxel

Tumor boundary
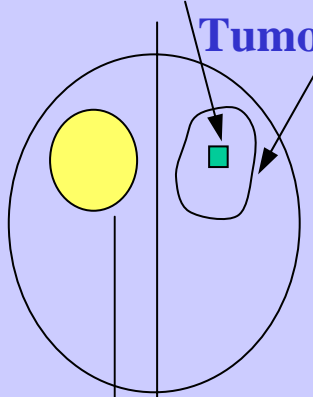
Null distribution

•To assess the MIC value of a voxel near the tumor, Null distribution is estimated from MIC values of an appropriate region in the contra-lateral hemisphere

•We then assess the statistical significance of the MIC value at the target voxel using this null distribution with an appropriate procedure for multiple comparisons.

The images below show MIC values statistically thresholded with this procedure.
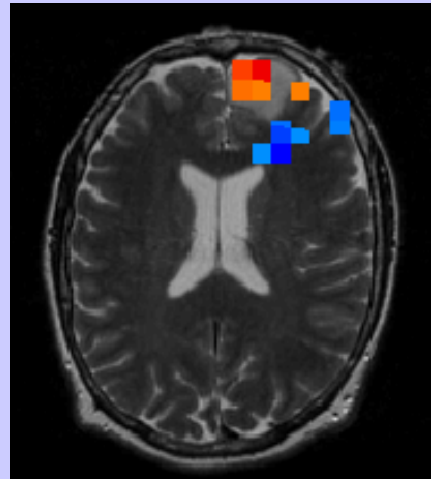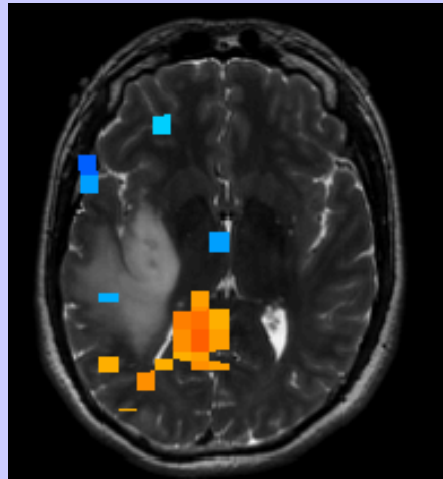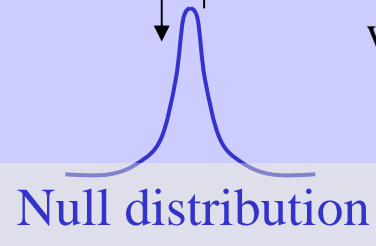
High connectivity
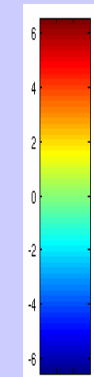
Low connectivity

•This statistical assessment can also provide information on regions with abnormally low connectivity, as well as regions with abnormally high connectivity.

•Abnormal values of mean imaginary coherence are found within tumor and near tumor boundary

Mean imaginary coherence mapping of schizophrenia patients (from alpha-band resting state MEG)

- Next example is mean imaginary mapping applied to schizophrenia patients. In this application, we use a group comparisons between the patient and control normal subject.

- This statistical procedure is called p-image analysis.

- Images below show the results from the statistical comparisons. Here, non-parametric unpaired t test was used. Increased connectivity regions are shown in red, and decreased connectivity regions are shown in blue.
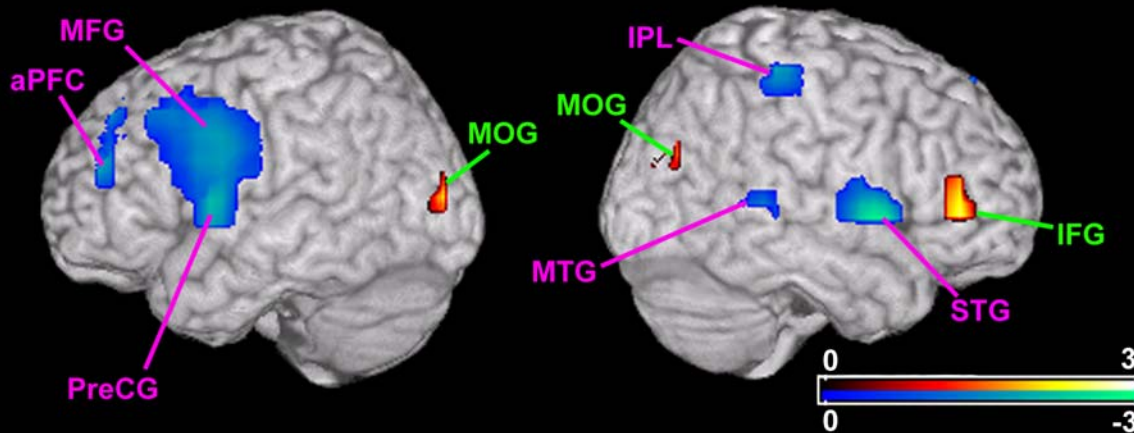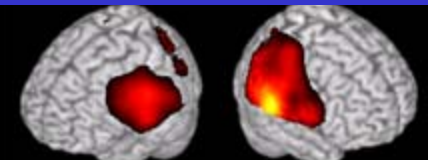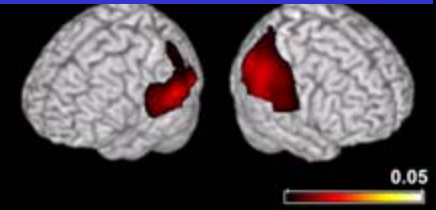
The greater connectivity regions are the right inferior frontal gyrus (IFG) and medial occipital gyrus (MOG) bilaterally. Reduced connectivity is observed near anterior prefrontal cortex (aPFC) and cortex along the medial frontal gyrus (MFG) and pre-central gyrus (PreCG) in patients with schizophrenia.

Correlations between MIC and symptom scores of schizophrenia patients

A) PANSS-E: Positive Symptoms

Left BA40

Right BA13
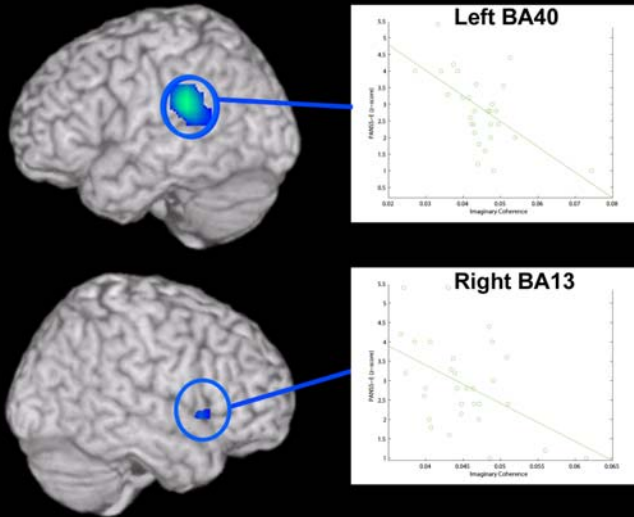
B) PANSS-E: Negative Symptoms

Left BA10
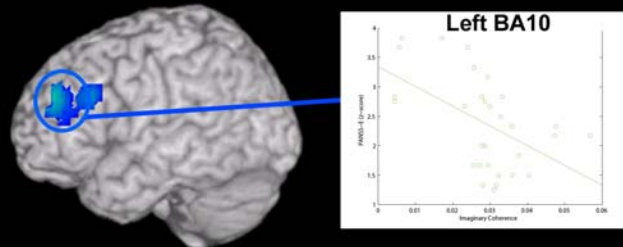
C) Depressed Symptoms

Anterior Cingulate
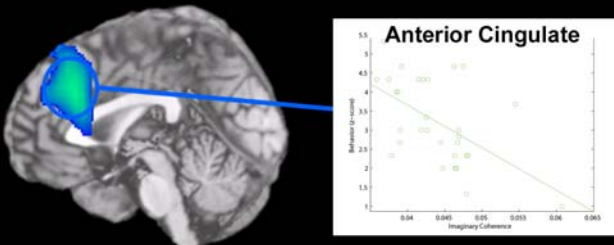
A correlation of MIC-value of individual patient and patient's symptom score are found.

• Brodmann's Area 40 and Brodmann's Area 13 are negatively correlated with positive symptoms assessed in the patients.

• Brodmann's Area 10 in left PFC is significantly correlated with negative symptoms.

• Low MIC values in a large region of cortex along the medial wall are associated with high ratings for depression in patients.

These results demonstrate that mean imaginary coherence imaging can be a powerful tool in psychopathology.

• positive symptoms: hallucinations, delusions & thought confusions
• negative symptoms: loss of interest, loss of energy, loss of warmth, loss of humor.

Mean imaginary coherence mapping for a patient with a traumatic brain damage

Blue parts indicate the brain regions with decreased mean imaginary coherence.
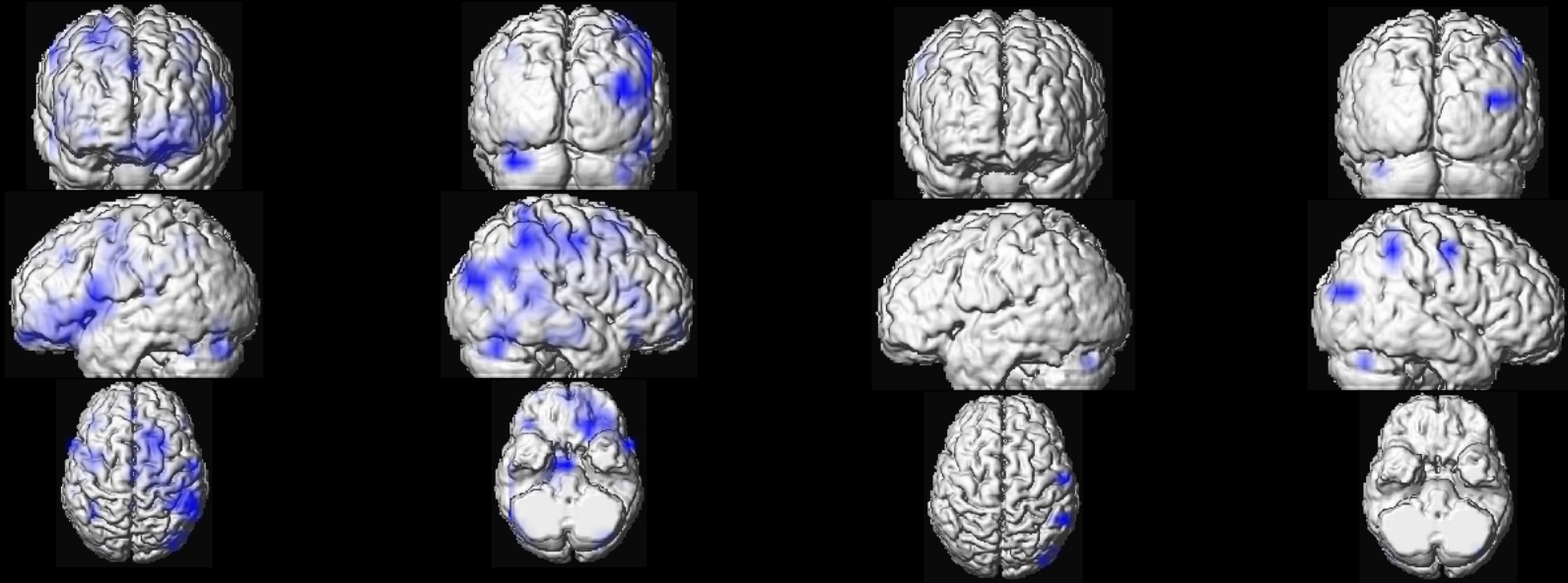
1 month after injury

2 years after injury

Blue-colored regions have significantly reduced in the 2-years-after results with still keeping the same structural pattern.

These results indicate that mapping mean imaginary coherence can provide useful clinical information on brain damage.

Summary

•Our investigation on estimating brain functional connectivity is described.

•The method, a pair-wise computation of coherence measure using estimated voxel time courses, relies on high performance inverse methods. Two inverse algorithms we have developed are briefly described.

•The use of imaginary coherence and its effectiveness are described.

•Several preliminary results on the use of envelope coherence and phase-slope index are presented.

•Mapping of mean imaginary coherence, and its clinical applications are described.

Adaptive Spatial Filters for Electromagnetic Brain Imaging

Neural activity in the human brain generates coherent synaptic and intra-cellular currents in cortical columns that create electromagnetic signals which can be measured outside the head using magnetoencephalography (MEG) and electroencephalography (EEG). Electromagnetic brain imaging refers to techniques that reconstruct neural activity from MEG and EEG signals. Electromagnetic brain imaging is unique among functional imaging techniques for its ability to provide spatio-temporal brain activation profiles that reflect not only where the activity occurs in the brain but also when this activity occurs in relation to external and internal cognitive events, as well as to activity in other brain regions. Adaptive spatial filters are powerful algorithms for electromagnetic brain imaging that enable high-fidelity reconstruction of neuronal activity. This book describes the technical advances of adaptive spatial filters for electromagnetic brain imaging by integrating and synthesizing available information and describes various factors that affect its performance. The intended audience include graduate students and researchers interested in the methodological aspects of electromagnetic brain imaging.

Adaptive Spatial Filters for Electromagnetic Brain Imaging

Series in Biomedical Engineering

Kensuke Sekihara
Srikantan S. Nagarajan

Adaptive Spatial Filters for Electromagnetic Brain Imaging

Springer

Collaborators

University of California, San Francisco

Srikantan S. Nagarajan
Leighton Hinkley
Julia Owen
Hagai Attias
David Wipf
Adrian G. Guggisberg
Anne Findlay
Sussane Honma

Yokogawa Electric Ltd.

Hiroaki Tanaka
Eiichi Okumura

Thank you very much for your attention